Energy Decomposition Analysis for Metal Surface−Adsorbate Interactions by Block Localized Wave Functions

Ruben Staub,[†] Marcella Iannuzzi,[‡][ID] Rustam Z. Khaliullin,[¶][ID] and Stephan N. Steinmann[*][,†][ID]

[†]Univ Lyon, Ecole Normale Supérieure de Lyon, CNRS Université Lyon 1, Laboratoire de Chimie UMR 5182, 46 allée d'Italie, Lyon, F-69364, France

[‡]Institut für Chemie, University of Zurich, Winterthurerstrasse 190, Zurich, CH-8057, Switzerland

[¶]Department of Chemistry, McGill University, 801 Sherbrooke Street West, Montreal, Québec H3A 0B8, Canada

S *Supporting Information*

ABSTRACT: The energy decomposition analysis based on block localized wave functions (BLW-EDA) allows one to gain physical insight into the nature of chemical bonding, decomposing the interaction energy in (1) a "frozen" term, accounting for the attraction due to electrostatic and dispersion interactions, modulated by Pauli repulsion, (2) the variationally assessed polarization energy, and (3) the charge transfer. This method has so far been applied to gas- and condensed-phase molecular systems. However, its standard version is not compatible with fractionally occupied orbitals (i.e., electronic smearing) and, as a consequence, cannot be applied to metallic surfaces. In this work, we propose a simple and practical extension of BLW-EDA to fractionally occupied orbitals, termed Ensemble BLW-EDA. As illustrative examples, we have applied the developed method to analyze the nature of the interaction of various adsorbates on Pt(111), ranging from physisorbed water to strongly chemisorbed ethylene. Our results show that polarization and charge transfer both contribute significantly at the adsorption minimum for all studied systems. The energy decomposition analysis provides details with respect to competing adsorption sites (e.g., CO on atop vs hollow sites) and elucidates the respective importance of polarization and charge transfer for the increased adsorption energy of H_2S compared to H_2O. Our development will enable a deeper understanding of the impact of charge transfer on catalytic processes in general.
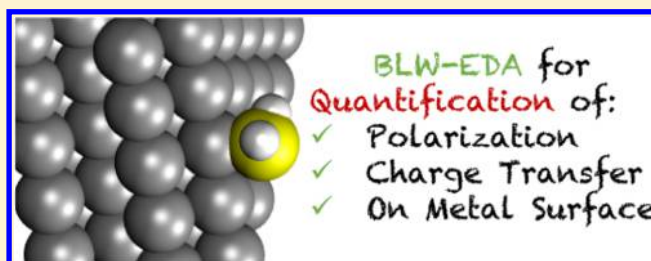
1. INTRODUCTION

Analyzing the chemical bond to understand the driving force and diversity of bonding is almost as old as quantum mechanics.[1,2] Bader's quantum theory of the atom in a molecule[3] and the natural bond orbitals by Weinhold et al.[4] are among the most popular approaches, but since the decomposition of the chemical bond energy into different contributions is not unique,[5] a multitude of other energy decomposition analysis (EDA) schemes have been developed.[6] All these different schemes come with their advantages and weaknesses, so that application of several tools can either bring contradicting results or provide confidence that at least the trend is captured accurately.[7] Most of these tools are developed having molecules in mind, and their application to the bonding between surfaces and adsorbates is comparatively rare.[8−11] As one of the few examples, Tonner and co-workers have demonstrated that EDAs on semiconducting surfaces can provide a deep understanding of coverage effects[12] and elucidate peculiar bonding mechanisms.[13] Our goal is to extend the EDA based on the block localized wave function (BLW)[14,15] to metallic surfaces. The BLW is designed to localize the electrons in Hilbert space in the Mulliken sense, i.e., in terms of atom-centered basis functions. A typical choice is to restrict the expansion to basis functions of atoms of a

given molecule and thus exclude contributions from all other basis functions in the system, thus defining one block per molecule. The BLW, also known in this context as absolutely localized molecular orbitals (ALMO), is variationally optimized, and the different blocks polarize each other. The main advantage of the BLW-EDA compared to other EDAs is that the polarization of fragments in their mutual presence is computed fully variationally. This allows one to rigorously separate the polarization energy from charge transfer. The charge transfer in BLW-EDA includes bonding orbital interactions between the fragments, which distinguishes it from the charge transfer obtained by constrained density functional theory (CDFT),[16,17] where the charge transfer is defined in real space, rather than Hilbert space.[18]

The formulation of the theoretical framework exploited for optimizing the BLW goes back to the works of Stoll et al.,[19] who aimed at reducing the computational cost of the self-consistent field (SCF) procedure by using ALMOs. The variational optimization of blocks that are localized in Hilbert space has found other applications over the years, exploiting other properties of the BLW unrelated to computational

speed-ups. For instance, BLW has been proposed to be used to remove the basis set superposition error (BSSE),[20,21] and BLW-EDA has been applied to molecular complexes at the DFT[22−24] or correlated wave function level of theory,[25,26] quantifying hyperconjugation,[27,28] strain energies,[29] and even covalent bonds.[30,31] Furthermore, ALMOs can provide transferable molecular orbitals (where they are also called ELMOs for extremely localized molecular orbitals)[32−35] or fragment densities to be used in X-ray structure elucidations.[36] Through its variational character, BLW also provides the unique opportunity to directly assess the impact of electron delocalization on the properties of molecules by comparing computed NMR chemical shifts[37,38] and J-couplings[39] for (de)localized states, which can be seen as the comparison between a single Lewis structure and the true, electron delocalized state. Similarly, the electronic structure of the electron localized state can be analyzed by scalar fields such as the electron localization function (ELF) or the localized orbital locator (LOL) in order to shed more light on the consequences of electron delocalization on the electronic structure.[40,41] Due to the variational definition of the polarization energy, other applications involve investigation of the impact of polarization on the hydration shell of ionic solutes[42] and comparison between the BLW polarization energy and polarizable force fields, which has also been exploited to parametrize first-principles based force fields.[43,44]

Heterogeneous catalytic reactions involving metal surfaces or particles are involved in many major industrial processes, such as selective hydrogenations in refineries, ammonia synthesis, steam reforming, etc. Furthermore, metal catalysts are key in heterogeneous electrocatalysis, which is the technology used in electrolysis, fuel cells, and CO_2 reduction but also the synthesis of fine chemicals.[45] Therefore, analysis of the interaction of adsorbates with metallic surfaces can provide valuable insights for the design of novel, more efficient catalysts. Furthermore, when considering metal alloys, the difference between electronic and ensemble effects is a widely discussed topic.[46] BLW would allow one to construct an electron localized (neutral) state of a given secondary element, clearly resolving the electronic (charge transfer between the two metals) and ensemble effect.

The formulation of BLW is based on the assumption of doubly occupied orbitals, although extensions to spin-unrestricted systems exist,[47,48] where the system is assumed to have a gap between the highest occupied molecular orbital (HOMO) and the lowest unoccupied molecular orbital (LUMO). Metallic electronic structures are, instead, characterized by a continuum of energy levels over the Fermi energy, leading to partially occupied states.

In this work, we propose an extension of the BLW approach based on a mean field approximation, to which we refer to as Ensemble BLW-EDA. In the following, we first present the conventional SCF procedure for metallic systems, followed by the main notions of BLW. Then, we combine the two, extending BLW to metallic systems. Finally, we provide computational details and applications to the prototypical adsorption of molecules (H_2O, H_2S, C_2H_4, and CO) on Pt(111).

2. METHODOLOGY

2.1. Ensemble DFT. The ground state of a metallic system, i.e., where the density of states around the Fermi level is continuous, cannot be described by a single quantum state.

Rather, an ensemble of states is required, both for a physically sound description and for a smooth convergence of the wave function optimization in a self-consistent field (SCF) process. The different quantum states within the ensemble are weighted according to their probability in order to determine observables. Let $\hat{A}$ be an operator, and Ω is the set of all possible quantum states of a given system. Then, the expectation value $\langle A \rangle_\Omega$ of the ensemble is

$$\langle A \rangle_\Omega = \sum_{\chi \in \Omega} \langle \Psi_\chi | \hat{A} | \Psi_\chi \rangle p_\chi \tag{1}$$

where Ψ_χ is the wave function associated with the quantum state χ. Ψ_χ spans the ground- and single excited-state determinants of the system. p_χ is the probability that the real system is in the quantum state χ, based on the energy of χ.

In the present context, we are interested in the reformulation of the 1-electron density operator $\hat{\rho}$. In the Hartree−Fock approximation and in the case of orthonormal molecular orbitals ψ_i, $\hat{\rho}$ can be written as

$$\hat{\rho} = \sum_{occ\psi_i \in \Psi} |\psi_i\rangle\langle\psi_i| \tag{2}$$

Dealing explicitly with ensembles is computationally inefficient and would require dedicated implementations. Since singly excited determinants do not overlap with the ground-state determinant, the same set of molecular orbitals can be used to construct all the relevant quantum states of the system. Therefore, the ensemble 1-electron density ($\langle\hat{\rho}\rangle_\Omega$) can be written in a convenient manner by considering the population of the orbitals (also known as occupation numbers, n_i) instead of the probability of quantum states:

$$\langle\hat{\rho}\rangle_\Omega = \sum_{\chi \in \Omega} p_\chi \hat{\rho}_\chi = \sum_{\chi \in \Omega} p_\chi \sum_{\psi_i \in \Psi_\chi} |\psi_i\rangle\langle\psi_i| \tag{3}$$

$$\langle\hat{\rho}\rangle_\Omega = \sum_i |\psi_i\rangle\langle\psi_i| n_i = \sum_i |\sqrt{n_i}\psi_i\rangle\langle\sqrt{n_i}\psi_i| = \sum_i |\psi_i'\rangle\langle\psi_i'| \tag{4}$$

where i is the sum over all molecular orbitals, i.e., solutions of the Fock equation. In eq 4, we have introduced the rescaled orbitals:

$$|\psi_i'\rangle = \sqrt{n_i}|\psi_i\rangle \tag{5}$$

which are particularly convenient computationally. The occupation number n_i is related to the probability for the orbital ψ_i to be occupied. For finite temperatures, they are determined on the basis of the energy ϵ_i of ψ_i, invoking Fermi−Dirac statistics:

$$n_i = \frac{1}{\exp\left(\frac{\epsilon_i - \mu}{kT}\right) + 1} \tag{6}$$

where μ is the Fermi level, k is Boltzmann's constant, and T is the (electronic) temperature. With these rescaled orbitals $|\psi_i'\rangle$, the mixed-state 1-electron density R_Ω can be easily computed.

$$R_\Omega = \mathbf{CNC}^\dagger \tag{7}$$

where $\mathbf{C}$ is the molecular coefficient matrix and $\mathbf{N}$ is a diagonal matrix of Fermi weights n_i according to eq 6. Yang et al. have generalized this reformulation to any method that can be reformulated on the basis of the noninteracting Greens function, allowing one to apply the orbital scaling to virtual

orbitals and thus to compute correlation energies with MP2 or RPA for systems with fractional electrons.[49] With a mild approximation, these scaled orbitals can also be used for coupled cluster computations for systems with fractional electrons.[50]

2.2. BLW Formalism. The basic idea of the BLW formalism is to express the wave function of the system in terms of blocks of localized orbitals. In the present context, the orbitals are always localized on a subset of atoms, so that the BLW partitions the atom-centered basis functions in mutually exclusive blocks and imposes thereby a localization of the wave function in Hilbert space.

Formally, a block B_m is defined as a set of N_m basis functions $\{\phi_1^m...\phi_{N_m}^m\}$, such that each basis function is associated with exactly one block, i.e., $\Sigma_m N_m = N$, where N is the total number of basis functions of the system. In this work, the set of basis functions $\{\phi_1^m...\phi_{N_m}^m\}$ associated with the block B_m is the union of *all* N_j basis set functions $\{\phi_1^j...\phi_{N_j}^j\}$ used to describe the j_m atoms of B_m, so that $\Sigma_m j_m$ equals the total number of atoms in the system. Similarly, the electrons of the system are assigned to a given block. In our case, all blocks are neutral.

An ALMO is defined as a linear combination of basis functions associated with the same block. Therefore, an orbital ψ_{i^m} pertaining to block B_m is written:

$$|\psi_{i^m}\rangle = \sum_\nu C_{\nu,i}^m |\phi_\nu^m\rangle \tag{8}$$

where $\mathbf{C}$ is the orbital coefficient matrix for the entire system, while $\mathbf{C^m}$ is the matrix of block B_m. We have used greek letters to label atomic orbital basis functions and i^m indexes ALMOs of a given block B_m.

The global orbital coefficient matrix $\mathbf{C}$, which spans all molecular orbitals and, thus, has dimensions of $N \times N$, has a block-diagonal structure:

$$\mathbf{C} = \begin{pmatrix} \mathbf{C^1} & 0 & \cdots & 0 \\ 0 & \mathbf{C^m} & \cdots & 0 \\ \vdots & \vdots & \ddots & \vdots \\ 0 & 0 & \cdots & \mathbf{C^{\Sigma_m}} \end{pmatrix} \tag{9}$$

where $\mathbf{C^m}$ is the orbital coefficient matrix restricted to the block B_m. The orbital coefficients $C_{\nu,i}^m$ are variationally optimized according to the local diagonalization based SCF algorithm developed by Stoll et al.[19] and implemented in CP2K as the first stage of the two-step "ALMO-SCF" scheme.[51]

In general, both locality and orthogonality constraints cannot be satisfied simultaneously.[52] Therefore, ALMOs are inherently nonorthogonal between blocks, although they can be kept orthonormal within a block without loss of generality. In this study, we will work under this assumption. Hence, the ALMO overlap matrix (σ) has identity-like diagonal blocks but nonzero entries for overlaps between blocks.

In practice, the so-called reciprocal (or biorthogonal) occupied orbitals $|\tilde{\psi}_{i^m}\rangle$ are defined such that $\langle\tilde{\psi}_{i^m}|\psi_{j^l}\rangle = \delta_{i^m j^l}$:

$$|\tilde{\psi}_{i^m}\rangle = \sum_{l,j} |\psi_{j^l}\rangle \sigma_{i^m j^l}^{-1}, \quad \tilde{\mathbf{T}} = \mathbf{T}\sigma^{-1} \tag{10}$$

where l goes over all blocks and j^l indexes the occupied orbitals of block B_l; $\tilde{\mathbf{T}}$ is the coefficient matrix of reciprocal occupied

orbitals, and $\mathbf{T}$ is the occupied part of eq 9. To be explicit, $|\tilde{\psi}_{i^m}\rangle$ is expanded in terms of *all* basis functions of the system and not only of block B_m.

Reciprocal orbitals enable one to rewrite the Fock equations. As Stoll et al.[19] have demonstrated, the self-consistent solution of projected eigenvalue equations for each block is equivalent to finding variationally optimal ALMOs.

$$\hat{F}^m|\psi_{i^m}\rangle = \epsilon_i^m|\psi_{i^m}\rangle, \quad \hat{F}^m = (\hat{\mathcal{I}} - \hat{\rho} + \hat{\rho}^{m\dagger})\hat{F}(\hat{\mathcal{I}} - \hat{\rho} + \hat{\rho}^m) \tag{11}$$

$$\hat{\rho}^m = \sum_{i \in B_m} |\tilde{\psi}_{i^m}\rangle\langle\psi_{i^m}| = \sum_{l,\xi,\nu} R_{\xi\nu}^m|\phi_\xi^l\rangle\langle\phi_\nu^m| \tag{12}$$

where $\hat{\mathcal{I}}$ is the identity matrix, $\hat{F}$ is the conventional Fock operator, $\hat{F}^m$ is the Fock operator projected on block B_m, $\hat{\rho}$ is the density operator of the entire system, $\hat{\rho}^m$ is the non-Hermitian operator that represents the density of the block defined by using only ALMOs of block B_m, and R^m is the associated block density matrix. ν is a basis function of block B_m (see eq 8), while ξ indexes the atom centered basis function of blocks B_l.

At each SCF iteration, these projected Fock equations are solved independently for each block but coupled to each other between successive iterations due to the projection operators. In other words, each block B_m is optimized in the environment generated by all other blocks.

Since in mixed-state theory it is common to deal with orthonormal orbitals, we briefly discuss the connection between the use of reciprocal orbitals and a Lowdin orthonormalization:

$$|^L\psi_i\rangle = \sum_{occ\ j} |\psi_j\rangle \sigma_{ij}^{-1/2}, \quad {}^L\mathbf{T} = \mathbf{T}\sigma^{-1/2} \tag{13}$$

where i and j are general indexes of occupied orbitals, $\sigma^{-1/2}$ is the square root inverse of the overlap matrix, and $^L\mathbf{T}$ is the Lowdin orbital coefficient matrix. The 1-electron density is equivalently expressed through the Lowdin orthonormalized molecular orbitals and the use of reciprocal orbitals, the latter avoiding the expensive computation of $\sigma^{-1/2}$:

$$\hat{\rho} = \sum_{occ\ i} |^L\psi_i\rangle\langle^L\psi_i| = \sum_{occ\ i} |\tilde{\psi}_i\rangle\langle\psi_i| = \sum_{occ\ i} \sum_{\nu,\xi} \tilde{T}_{\nu i}|\phi_\nu\rangle\langle\phi_\xi|T_{\xi i}$$
$$= \sum_{\nu,\xi} \sum_{occ\ i} T_{\xi i}\tilde{T}_{i\nu}^\dagger|\phi_\nu\rangle\langle\phi_\xi| = \sum_{\nu,\xi} R_{\nu\xi}|\phi_\nu\rangle\langle\phi_\xi| \tag{14}$$

$$\mathbf{R} = {}^L\mathbf{T}{}^L\mathbf{T}^\dagger = \mathbf{T}\tilde{\mathbf{T}}^\dagger = \mathbf{T}(\mathbf{T}\sigma^{-1})^\dagger = \mathbf{T}\sigma^{-1}\mathbf{T}^\dagger \tag{15}$$

where $\mathbf{R}$ is the conventional 1-electron density matrix. $\mathbf{R}$ can then be fed to standard routines to determine the electron density in real space, compute gradients, and so forth.

2.3. Ensemble BLW. *2.3.1. Exact Ensemble Formulation.* In order to adapt the BLW formalism to an ensemble formulation, we need to adapt the density matrices $\mathbf{R}$ or, equivalently, the construction of the reciprocal orbitals (eq 10). In other words, we apply the general formula (eq 3) for the computation of an ensemble density matrix $\mathbf{R_\Omega}$ to nonorthogonal molecular orbitals:

$$\mathbf{R}_\Omega = \sum_{\chi \in \Omega} p_\chi \mathbf{T}_\chi = \sum_{\chi \in \Omega} p_\chi \mathbf{T}_\chi \sigma_\chi^{-1} \mathbf{R}_\chi^\dagger$$

$$= \sum_{\chi \in \Omega} p_\chi \mathbf{T}_\chi (\mathbf{T}_\chi^\dagger \mathbf{S} \mathbf{T}_\chi)^{-1} \mathbf{T}_\chi^\dagger \tag{16}$$

where p_χ is the probability that the real system is in the quantum state χ, $\mathbf{R}_\chi$ is the density matrix of this quantum state, $\mathbf{T}_\chi$ is the occupied orbital coefficient matrix associated with the wave function Ψ_χ, σ_χ^{-1} is the overlap matrix of the quantum state χ, and $\mathbf{S}$ is the basis set function overlap matrix which is common for all quantum states, since it is a property of the geometry and basis set.

Let us consider a general orbital coefficient matrix $\mathbf{C}$ containing all the localized orbitals used to construct every $\mathbf{T}_\chi$, the occupied orbital matrix of quantum state χ. Therefore, one can construct any $\mathbf{T}_\chi$ from $\mathbf{C}$:

$$\mathbf{T}_\chi = \mathbf{C}\Delta_\chi = \mathbf{C}\begin{pmatrix} \delta_{1\chi} & 0 & \cdots & 0 \\ 0 & \delta_{2\chi} & \cdots & 0 \\ \vdots & \vdots & \ddots & \vdots \\ 0 & 0 & \cdots & \delta_{n+k\chi} \end{pmatrix}, \quad \delta_{i\chi} = \begin{cases} 1 & \text{if } \psi_i \in \Psi_\chi, \\ 0 & \text{otherwise} \end{cases} \tag{17}$$

where Δ_χ can be seen as a rescaling matrix with a dimension of $N \times N$.

Combining eq 17 with eq 16, we obtain the following reformulation:

$$\mathbf{R} = \sum_{\chi \in \Omega} p_\chi \mathbf{R}_\chi = \sum_{\chi \in \Omega} p_\chi \mathbf{T}_\chi \sigma_\chi^{-1} \mathbf{T}_\chi^\dagger = \sum_{\chi \in \Omega} p_\chi \mathbf{C}\Delta_\chi \sigma_\chi^{-1} \Delta_\chi \mathbf{C}^\dagger$$

$$= \mathbf{C}\left(\sum_{\chi \in \Omega} p_\chi \Delta_\chi \sigma_\chi^{-1} \Delta_\chi\right)\mathbf{C}^\dagger = \mathbf{C}^\Omega \sigma^{-1} \mathbf{C}^\dagger \tag{18}$$

where $^\Omega\sigma^{-1} = \sum_{\chi \in \Omega} p_\chi \Delta_\chi \sigma_\chi^{-1} \Delta_\chi$.

Equation 18 requires σ_χ^{-1} to be computed for each state involved separately; i.e., it is not an efficient reformulation of eq 16. This contrasts with the canonical case, where eq 4 provides an efficient reformulation of eq 3, since the different quantum states involved are orthonormal among each other.

If we have k orbitals in addition to the n formally doubly occupied orbitals, then the maximum number $|\Omega|$ of quantum states to evaluate eq 17 is

$$|\Omega| = \binom{n+k}{n} = \frac{(n+k)!}{n!k!} \tag{19}$$

In the worst case, $k = n$, $|\Omega| \approx \frac{2^{2n}}{\sqrt{\pi n}}$; i.e., the number of states to be considered is exponential in n. Hence, such a method is not applicable to sizable systems (e.g., a little more than 7×10^{201} states for the Pt(111) surface investigated in the later sections).

Why can there not be a simple reformulation of ensemble BLW, just like in the canonical case? Considering eq 14, we can understand that ALMOs are treated as if they would be orthonormalized when computing the density matrix. Therefore, scaling them by their occupation number is not an option, since this lack of normalization will simply be offset by the corresponding σ^{-1}. A second point of interference when aiming at a simplified ensemble description comes from the interdependence of blocks. Let us consider a two block system. According to eq 10, the reciprocal orbitals of block 1 depend on the occupied orbitals of all blocks. Hence, in general (i.e., when the orbitals between blocks overlap), varying the

occupations in block 2 results in a varying environment for block 1 (and vice versa). In other words, the different quantum states in block 1 are subjected to different environments, depending on the quantum states of block 2. To put this in mathematical terms, let us consider two quantum states χ and χ', with associated wave function Ψ_χ and $\Psi_{\chi'}$ and three different orbitals ψ_1, ψ_2, and ψ_3 (considered doubly occupied) such that $\{\psi_1, \psi_2\} \subseteq \Psi_\chi$ and $\{\psi_1, \psi_3\} \subseteq \Psi_{\chi'}$ but $\psi_3 \notin \Psi_\chi$ and $\psi_2 \notin \Psi_{\chi'}$. If we would like to use the same set of ALMOs for describing Ψ_χ and $\Psi_{\chi'}$, then we would like $\tilde{\psi}_1$ to be equal to $\tilde{\psi}_1'$ (respectively, the reciprocal orbital of ψ_1 computed in the quantum state χ and χ'), so that eq 18 can be simplified in full analogy with the situation when using orthonormalized orbitals. However, the reciprocal orbital $\tilde{\psi}_1$ in the quantum state χ does not change by replacing the orbital ψ_2 by ψ_3, if and only if ψ_1 does not overlap with neither ψ_2 nor ψ_3 and there exists no $\psi_i \notin \{\psi_1, \psi_2, \psi_3\}$ in any quantum state $\chi_j \in \Omega$ such that both ψ_1 and ψ_2 (or ψ_3) overlap with ψ_i:

$$|\tilde{\psi}_1\rangle = |\tilde{\psi}_1'\rangle \Leftrightarrow \begin{cases} \langle \psi_1 | \psi_2 \rangle = 0 \\ \wedge (\,\forall\, \chi \in \Omega,\, \nexists \psi_i \in \Psi_\chi \backslash \{\psi_1, \psi_2\}, \\ \quad \psi_1 \in \Psi_\chi \rightarrow (\langle \psi_1 | \psi_i \rangle \neq 0 \wedge \langle \psi_2 | \psi_i \rangle \neq 0)) \\ \wedge (\text{idem for } \psi_3 \text{ instead of } \psi_2) \end{cases} \tag{20}$$

Therefore, the occupation-state dependency of the orthonormalized orbitals is always present, except when the added or removed orbitals do not overlap with the rest of the system. Due to this occupation-state dependency of the orthonormalized orbitals, they cannot be used to construct an ensemble density matrix by rescaling them, in contrast to the canonical case.

As a conclusion, since the orbitals are nonorthogonal, when an orbital occupation is modified, the whole system has to readapt. Note that this conclusion applies to the use of any nonorthogonal orbitals and not only to ALMOs.

2.3.2. Mean-Field Approximation to Ensemble BLW. The condition to formulate a computationally tractable approximation to ensemble BLW is that the contribution of each orbital to the ensemble density can be computed only once per SCF iteration and can then be weighted by the probability that the real system is in a quantum state containing this orbital (or equivalently, the probability that this orbital is occupied in the real system). In other words, we need to devise a scheme in which we have a common overlap matrix σ for all quantum states involved; i.e., we generate an average interaction field (over all quantum states) that is applied to every quantum state. Furthermore, we require that the scheme is equivalent to standard ensemble theory for a single block. This implies that eq 6 is applied to each block separately (with the block specific chemical potential μ^m), so that the total number of electrons in each block remains an integer. With these two requirements, we arrive at a mean-field approximation to the overlap matrix ($^\alpha\sigma$).

The interaction (i.e., overlap) between $|\psi_{i^m}\rangle$ and $|\psi_{j^l}\rangle$ from any block is rescaled by $\sqrt{n_i}\sqrt{n_j}$, while the self-overlap remains unmodified. This rescaling provides an approximate overlap matrix $^\alpha\sigma$:

$$^\alpha\sigma_{ij} = \begin{cases} \langle \psi_{i^m} | \psi_{i^m} \rangle = 1 \\ \langle \psi_{i^m} | \psi_{j^l} \rangle \sqrt{n_i}\sqrt{n_j} \end{cases} \tag{21}$$

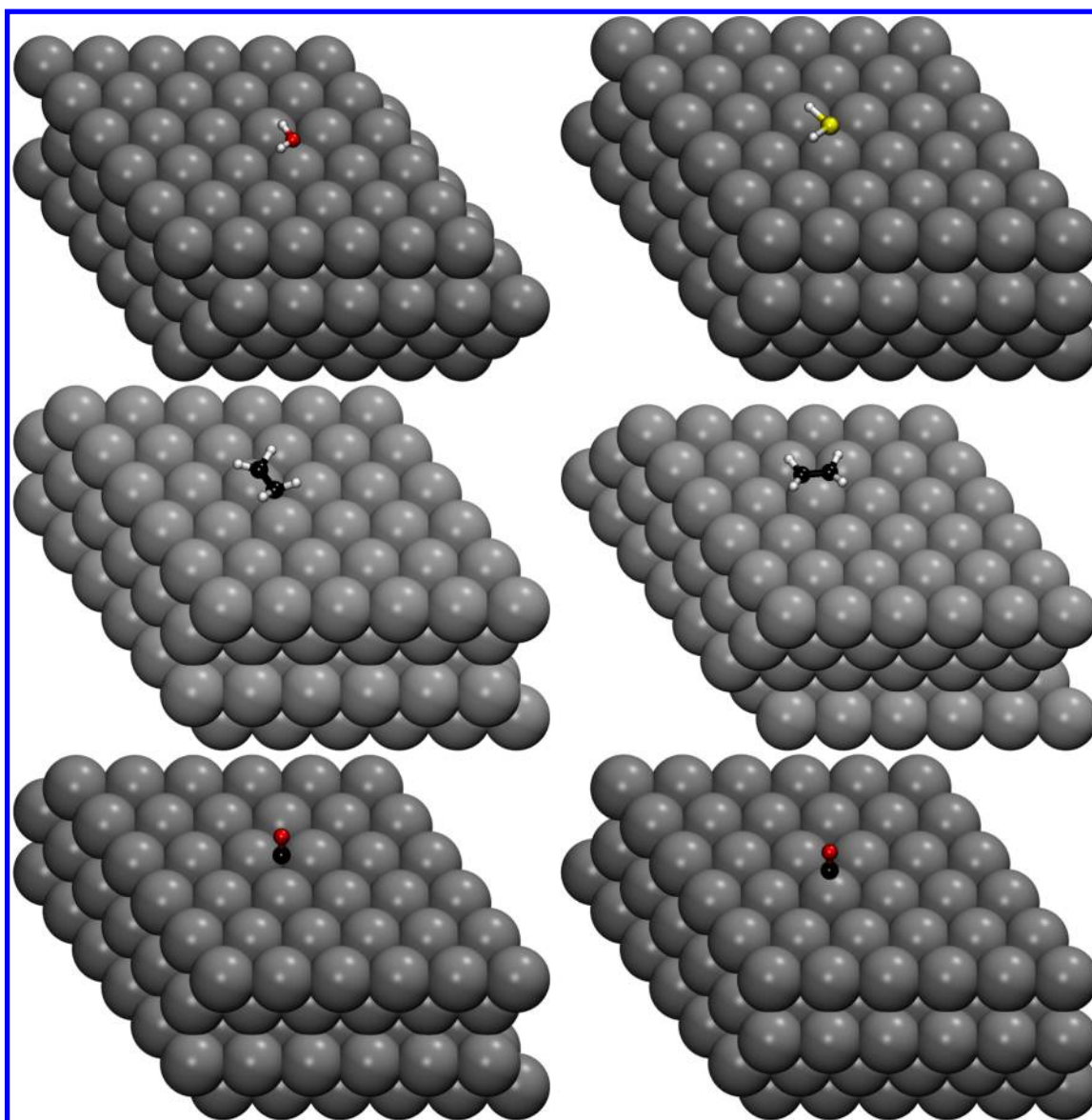Hence, the density matrix $^\alpha\mathbf{R}_\Omega$ can be written:

Figure 1. Top: H_2O (left) and H_2S (right) top adsorption on Pt(111). Middle: Ethylene adsorption in a di-σ (left) and π (right) adsorption mode. Bottom: CO on fcc (left) and top (right) adsorption sites. All images refer to the equilibrium distance with respect to the surface.

$$^{\alpha}\mathbf{R}_{\Omega} = \mathbf{T}'^{\alpha}\sigma^{-1}\mathbf{T}'^{\dagger} \tag{22}$$

where $\mathbf{T}'$ is the rescaled orbital coefficient matrix, in close analogy to eq 5, for the canonical case.

We use $|^{s}\psi_{i_m}\rangle$ to denote the presence of fractionally occupied ALMOs, i.e., the ones that necessitate the use of $^{\alpha}\sigma$. $|^{s}\psi_{i_m}\rangle$ has rescaled interactions (overlap), except with themselves. Therefore, we call them "selfish orbitals". Unlike the canonical rescaled orbitals, selfish orbitals cannot be considered "shrunk"; they just interact less with their environment:

$$\forall j \neq i \quad \langle^{s}\psi_{i_m}|^{s}\psi_{j_l}\rangle = \sqrt{n_i}\sqrt{n_j}\langle\psi_{i_m}|\psi_{j_l}\rangle; \text{ but } \langle^{s}\psi_{i_m}|^{s}\psi_{i_m}\rangle = \langle\psi_{i_m}|\psi_{i_m}\rangle \tag{23}$$

where j goes over ALMOs of all blocks.

In practice, at each SCF iteration, the orbital coefficients $\mathbf{T}$ are scaled according to the (updated) occupation number, yielding $\mathbf{T}'$. With these scaled coefficients, the overlap matrix σ is computed. Then, the diagonal of σ is set to unity to obtain $^{\alpha}\sigma$. The density matrix is computed using eq 22. In brief,

except for the use of $\mathbf{T}'$ and $^{\alpha}\sigma$, the SCF procedure by Stoll et al.[19] is not modified.

Please note that, for noninteracting systems (blocks that are far apart), the mean-field approximation reverts back to the canonical answer. Similarly, if the orbital occupations are either 0 or 2 (0 K limit of a system with a nonvanishing gap), our approximation provides the regular BLW result.

In our implementation in CP2K, we exploit the eigenvalue based optimization,[15,19] which has been implemented in CP2K[51,53] and allows a variational optimization of the ensemble BLW. The computational cost of the extension to partially occupied orbitals is negligible thanks to the use of selfish orbitals, and the additional storage used is limited to an array containing the orbital energies.

As discussed in the Supporting Information, the error introduced by the mean-field approximation turns out to lead to losses of electrons in the Ensemble BLW. For example, for H_2O, up to 0.005 electrons are lost when the molecule is closest to the metal surface. The energetic consequence on the polarization energy of this electron loss can be estimated to be

up to 0.5 kcal mol^{-1} assuming a metallic system with a typical work function of around 5 eV. As a result, the charge-transfer energy, which does not suffer from this electron loss, is slightly overestimated compared to the polarization energy. Given that water, which is the least strongly adsorbed molecule studied herein, has an adsorption energy of −9.7 kcal mol^{-1}, such an error is deemed acceptable. In all cases, no loss or a small loss of electrons is encountered, never a gain in electrons. This can be rationalized in analogy to Hartree−Fock, where the average electron repulsion overestimates the actual electron repulsion. Hence, our mean-field approximation is an upper bound to exact ensemble BLW. Since ensemble DFT formulation is variational with respect to the electronic free energy (i.e., when accounting for the entropy related to the fractionally occupied orbitals), our Ensemble BLW-EDA defines the charge transfer through a variational principle for the interaction of adsorbates with metallic surfaces.

3. COMPUTATIONAL DETAILS

The adsorbed structures were optimized with VASP 5.4.1[54,55] using periodic boundary conditions applying the reoptimized Perdew, Burke and Ernzerhofer (PBE) functional to make it compatible with the nonlocal van der Waals (vdW) functional, in short optPBE-vdW[56] functional, which is has been found to be, together with PBE-dDsC,[57] another dispersion corrected density functional, most accurate for adsorption energies on Pt(111),[58] and is available in CP2K, the code that is used for all Ensemble BLW-EDA computations. An energy cutoff of 400 eV is chosen for the expansion of the plane-wave basis set. The electron−ion interactions are described by the PAW formalism.[59,60] The p(6 × 6) unit cell is built from bulk platinum (2.821 Å nearest neighbor distance) with four metallic layers. Additional tests regarding the need for K-point sampling reveal that the Γ-point optimized geometries are very close to the ones obtained with a 3 × 3 × 1 K-point mesh. The adsorption energy at the Γ-point is overestimated by 1−5 kcal mol^{-1}, corresponding to up to 10% at the equilibrium distance (see Table S2). This accuracy is deemed acceptable for the current purpose, where the relative importance of different interaction energy components and their evolution as a function of the surface−adsorbate distance is analyzed. The out-of-plane vector of the unit cell was chosen to be ~23 Å to achieve a negligible interaction between periodic images.

In CP2K, the molecular orbitals were represented by a double-ζ Gaussian basis set with one set of polarization functions, called DZVP-MOLOPT-SR-GTH for both BLW-EDA and BSSE corrected SCF DFT simulations.[61] A cutoff of 400 Ry was used to describe the electron density. The exchange-correlation (XC) energy was approximated with the optPBE-vdW[56] functional. The Brillouin zone was described at the Γ-point. Goedecker, Teter and Hutter (GTH) pseudopotentials[62] based on the PBE functional were used to describe the interactions between the valence electrons and the ionic cores, and the electronic smearing was approximated by a Fermi−Dirac distribution at 300 K, applied to all computations.

Figure S1 provides a comparison between the total interaction energy (ΔE_{int}, vide infra, eq 24) as computed by standard KS-DFT with VASP and CP2K. In both codes, we compare a 10 and a 18 valence electron pseudopotential. The 18 valence electron potential of CP2K gives interaction energies very close to the one provided by VASP, independently if the latter uses 10 or 18 valence electrons.

3.1. Energy Decomposition Analysis.

The newly extended EDA scheme is now applied to charge transfer analysis of adsorption at a metallic surface. We select three prototypical couples of systems (see Figure 1), aiming at describing different types of bonding. The first couple is H_2O and H_2S, for which no strong bond formation is expected, although H_2S is interacting more strongly with Pt(111) than water. The second couple compares the di-σ and π adsorption modes of ethylene, while the third couple investigates the difference between CO adsorbed on fcc and top sites.

For all these systems, we have computed the interaction energy as a function of the distance between the surface and the adsorbate. All coordinates are fully optimized, except the z-coordinate of the heavy atoms closest to the surface and the two bottom layers that are kept fixed in their bulk position. We define the total interaction energy ΔE_{tot} as

$$\Delta E_{tot} = E_{system} - E_{frag\,1,opt} - E_{frag\,2,opt} - \Delta E_{BSSE} \quad (24)$$

where E_{system} is the standard KS-SCF energy of the full system and $E_{frag,opt}$ is the corresponding energy of the freely optimized fragments. Since the BLW is only defined in a localized basis set, we have to correct for the basis set superposition error (BSSE), which we do according to the counterpoise procedure of Boys and Bernardi,[63] giving rise to the energy correction ΔE_{BSSE}. Note, however, that BSSE only affects the charge-transfer term, as all other terms are evaluated using exclusively the fragment basis set.

For the energy decomposition analysis, each system is divided into two blocks: a metallic block containing the metal surface and an adsorbate block containing the adsorbed molecule. As common in BLW-EDA,[22,23,64] we decompose the total interaction energy ΔE_{tot} into the following terms: preparation or deformation (ΔE_{deform}), the frozen energy term (ΔE_{frozen}) that describes the interaction of the two isolated fragment densities brought together and covering electrostatic interaction and Pauli repulsion[22] as well as dispersion interactions,[64] polarization (ΔE_{pol}) energy, obtained by variationally optimizing the BLW, and finally, the charge transfer (ΔE_{CT}) interaction that includes covalent bond formation.

$$\Delta E_{tot} = \Delta E_{deform} + \Delta E_{frozen} + \Delta E_{pol} + \Delta E_{CT} \quad (25)$$

These terms can be expressed as

$$\Delta E_{deform} = E_{frag\,1,sys} - E_{frag\,1,opt} + E_{frag\,2,sys} - E_{frag\,2,opt} \quad (26a)$$

$$\Delta E_{frozen} = E_{guess} - E_{frag\,1,sys} - E_{frag\,2,sys} \quad (26b)$$

$$\Delta E_{pol} = E_{BLW} - E_{guess} \quad (26c)$$

$$\Delta E_{CT} = E_{system} - E_{BLW} - \Delta E_{BSSE} \quad (26d)$$

where $E_{frag,sys}$ corresponds to the energy of a fragment in its final geometry adopted in the presence of the other fragment. E_{guess} is the systems energy obtained by a superposition of the fragment density matrices, which corresponds to the "frozen" density interaction energy approximation. E_{BLW} is the energy obtained by Ensemble BLW.

4. RESULTS AND DISCUSSION

As a first application of Ensemble BLW-EDA to metal surfaces, we compare the adsorption of H_2O and H_2S on Pt(111). As shown in Figure 1 for both molecules, the most favorable
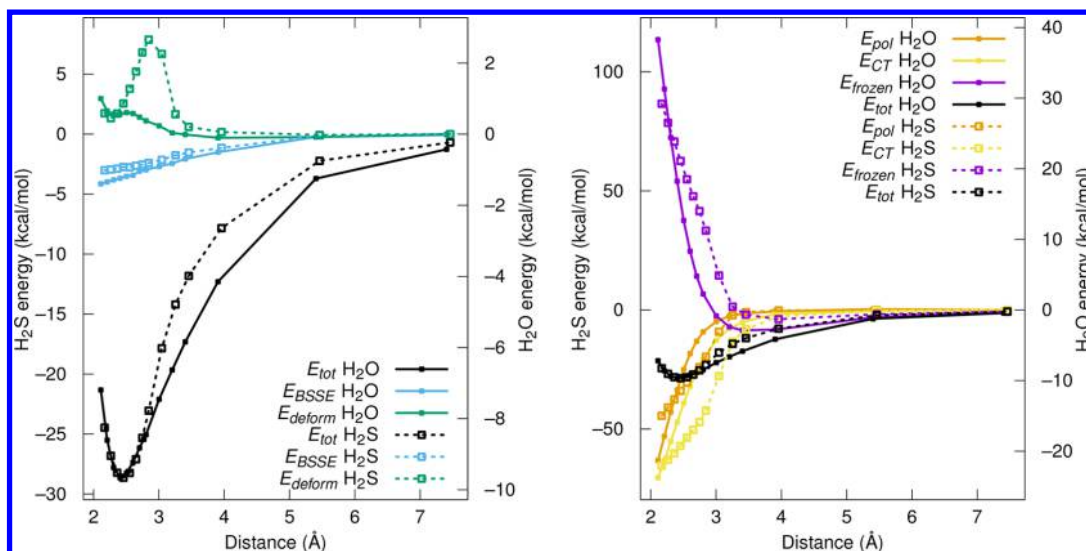
Figure 2. Energy decomposition analysis for H_2O (solid lines, right y-axis) and H_2S (dashed lines, left y-axis). The total interaction energy is compared to the BSSE and the deformation energy on the left, while the right quantifies the frozen monomers, polarization, and charge transfer interaction energy. Note that the y-scales are aligned in such a way that the equilibrium interaction energy and the zero interaction energy are aligned for both systems; see Supporting Information for separated figures.

adsorption configuration is atop, with the molecular plane approximately parallel to the surface. The total interaction energy as a function of the Pt−O or Pt−S distance shows that, despite the nominally larger noncovalent radius of sulfur with respect to oxygen (1.8 and 1.5 Å according to Bondi[65]), the minimum is found around 2.4 Å in both cases. This can be rationalized by the overall stronger interaction of Pt−H$_2$S (29 kcal mol^{-1}) compared to Pt−H$_2$O (9 kcal mol^{-1}), which allows S to approach the surface more closely than O with respect to its size. The BSSE contribution to the interaction energy is similar for H$_2$O and H$_2$S (roughly 10% of the total interaction energy). Therefore, the comparison between the two systems could be performed with a 10% accuracy without the BSSE correction, for instance for molecular dynamics simulations of H$_2$S dissolved in water. The deformation energy of the two systems show different patterns. While the energetic cost to deform water/Pt(111) to its optimal geometry is very small (at most 0.5 kcal mol^{-1}), H$_2$S/Pt(111) undergoes a deformation up to 7 kcal mol^{-1} at a distance that is only slightly longer than the equilibrium distance, while it drops at shorter distances to about 1 kcal mol^{-1}. Analyzing the origin of the deformation energy, we identify the deformation of the metal surface as the major contributor. As shown in Figure S2, the Pt atom, on which the adsorbate is adsorbed, is "pulled out" of the surface at intermediate distances. After a certain elongation, it goes back to the original position, almost as if the spring had been overstretched and thus broken. Moving to the interaction energy components of the fragments after paying the preparation (deformation) energy (right-hand graph of Figure 2), we first observe that the "frozen" term, i.e., the energy cost (or gain) of putting the fragments together without electronic density changes, follows the expected increase in atomic size when replacing oxygen by sulfur: The energy of assembly becomes positive for distances below 2.8 and 3.2 Å for H$_2$O and H$_2$S, respectively. At larger distances, the interaction energy is already negative without any further electronic relaxation. This is due to the subtle balance between Pauli repulsion and attraction by dispersion interactions. Note that electrostatic interactions are also included at this stage, but

since the isolated metal surfaces do not have significant electrostatic moments (dipole, quadrupole, etc.), it barely contributes in the present systems. Allowing the electron density to relax in the presence of the other fragment, but prohibiting any charge transfer or direct orbital interaction, affords the stabilizing polarization energy ΔE_{pol}. H$_2$S has a 2.7 times larger polarizability than H$_2$O (26.7 and 9.8 au^3, respectively,[66]). Indeed, there is roughly a factor of 3 between ΔE_{pol} for H$_2$S compared to H$_2$O at all relevant distances (>2.3 Å), in close agreement with the corresponding factor for the total interaction energy. The charge transfer between the metal surface and the adsorbate is, however, much more important for H$_2$S than for H$_2$O. This contrasting energy decomposition can be rationalized recalling that sulfides are softer bases than oxides and that platinum is a soft acid. Furthermore, interactions with sulfur can benefit from stabilization through hypervalence by increasing the ionic character of bonds.[67]

As a conclusion, the stabilizing interaction of a single water molecule with Pt(111) is due to equal amounts of polarization and charge transfer. In other words, even in this case of rather weak physisorption, the use of a polarizable force field is unlikely to be enough to capture the physics of the interaction energy accurately. However, a good approximation can be obtained since the two components are well correlated; i.e., counting the polarization energy twice, BLW could capture a reasonable approximation of the total interaction energy. This insight might help the development of more accurate Pt/H$_2$O force fields.[68,69] The situation for H$_2$S is more challenging to approximate: charge transfer dominates the interaction energy, which also induces significant deformations of the surface. Hence, already for H$_2$S adsorption, explicit terms to mimic orbital/charge-transfer interactions are required. The situation can be simplified by excluding surface deformation. Given the scarcity of accurate force fields for the deformation of metal surfaces, this is the preferred setup anyway. Figure S3 shows that on an ideal surface the deformation energy is negligible and the charge-transfer and polarization energies are now as smooth as for water. Furthermore, on an ideal surface, a very similar relative importance of the various contributions is
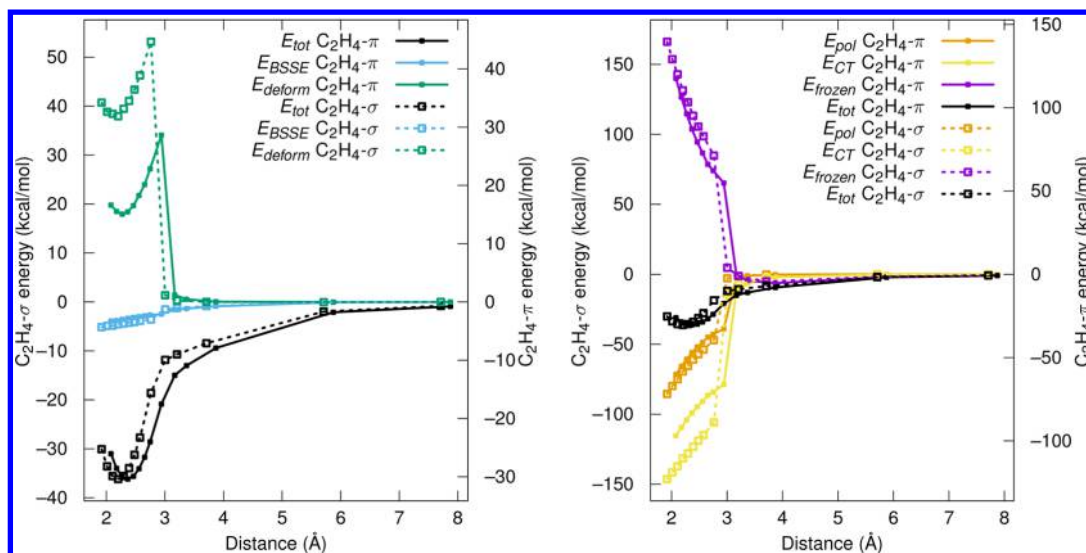
Figure 3. Energy decomposition analysis for di-σ (dashed lines, left y-axis) and π (solid lines, right y-axis) C_2H_4. The total interaction energy is compared to the BSSE and the deformation energy on the left, while the right quantifies the frozen monomers, polarization, and charge-transfer interaction energy.
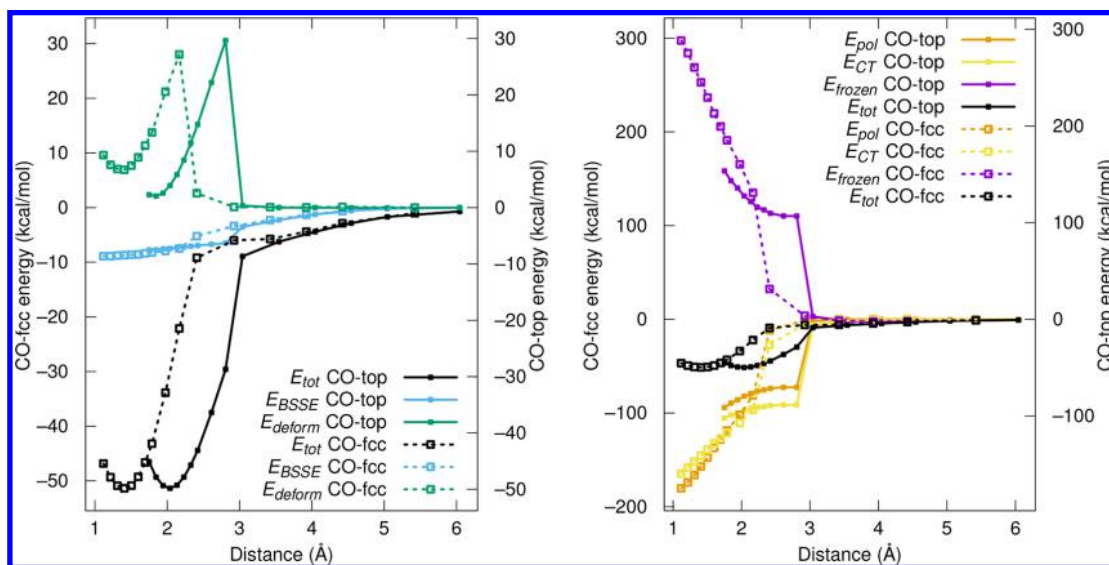

Figure 4. Energy decomposition analysis for top (solid lines, right y-axis) and fcc (dashed lines, left y-axis) CO on Pt(111). The total interaction energy is compared to the BSSE and the deformation energy on the left, while the right quantifies the frozen monomers, polarization, and charge transfer interaction energy.

obtained for H_2O and H_2S. Since ΔE_{tot} is not very different when using an ideal Pt(111) surface, H_2S adsorption can be described without taking into account the surface deformation with only a small loss in accuracy. Given that ΔE_{CT} is most strongly affected, this analysis also identifies the charge transfer as the origin of the deformation.

On a more technical level, we have also investigated the influence of the electronic smearing temperature on the results. In Figure S4, we show that increasing the electronic temperature from 300 to 1000 K does not visibly affect the results. Even at 2000 K, only changes of 3−4 kcal mol^{-1} are observed, leaving the relative importance of different terms unchanged. As detailed in the Supporting Information, the small changes observed can be rationalized keeping in mind that higher electronic temperatures lead to the occupation of orbitals lying above the Fermi level.

The deformation energy observed for H_2S is small compared to the one obtained for ethylene adsorption (see Figure 3). This does not come as a surprise, given that the adsorbed geometry (Figure 1) suggests a rehybridization of the sp^2 carbon atoms. This significant geometric rearrangement is best associated with a "state crossing": sp^2 at long distances but ~sp^3 at short distances. This state-crossing is noncontinuous, as best seen in the deformation energy, although other interaction energy components show a similar discontinuity. As mentioned above, the deformation is mainly due to the deformation of the metal surface, where the Pt atom is partially lifted out of the surface (see Figure S2). The BSSE is again in the order of 10% of the total interaction energy around the minimum, and the total interaction energy is, with 30 and 37 kcal mol^{-1} for π and di-σ, respectively, similar. Furthermore, the larger geometric deformation (H−C−C−H dihedral angles of 132° and 156°) for the di-σ mode compared to the π mode

is nicely captured by the deformation energy. Similar to H_2S, the maximum deformation energy is obtained when the molecule is close enough to the surface to actually "feel" it but not close enough to form strong covalent bonds. The deformation and the total interaction energy reflect quite well that the π mode approaches the surface less closely than the di-σ mode (Pt−C distance of 2.20 Å in π and 2.13 Å in di-σ). The right-hand side of the graph provides a rationalization: the Pauli repulsion (contained in E_{frozen}) is longer-ranged for the π bond, at the top of a Pt atom, than between the bridge site and carbon atoms that are not strictly on top of Pt atoms. The same observation also applies to the polarization and charge-transfer energy. However, the relative importance of repulsion, polarization, and charge transfer is surprisingly similar for both modes, demonstrating that the nature of the bonding interaction is the same. Nevertheless, the di-σ mode maximizes this bonding type which is characterized by ~40% polarization energy and ~60% charge transfer, very similar to the interaction of H_2S with the same surface.

The last example we are discussing here is the classic case of CO adsorption on Pt(111). One of the challenging questions is whether CO is adsorbed on top or on bridge/hollow sites and how this evolves as a function of the surface charge.[70] The following analysis investigates exclusively the bonding patterns at the respective adsorption sites, without drawing any conclusions, neither on the reliability of the chosen density functional nor on the actual site preference of CO on Pt(111).

In Figure 4, the data for CO adsorption on top and fcc sites is compared. At our level of theory, the fcc adsorption site is slightly preferred (−52 vs −49 kcal mol^{-1}). However, these graphs show very clearly the contrasting behavior of CO on these two sites: The top site experiences a significantly stronger Pauli repulsion, resulting in a longer equilibrium distance (2 Å compared to 1.5 Å). The deformation energy, on the other hand, is slightly lower at the equilibrium distance on the top site than on the fcc site, although the barrier for the state-crossing is roughly equal (~30 kcal mol^{-1}), shifted by 0.75 Å to longer distances for the top mode. Regarding the decomposition of the interaction energy, we can first note that the Pauli repulsion at long distances is lower for the fcc mode compared to the top adsorption mode but, at shorter distances, rises more quickly for the fcc site. Second, in contrast to the case of C_2H_4, the ratio of polarization and charge-transfer energy is quite different for the two adsorption modes. Somewhat surprisingly, the fcc mode shows a similar pattern as H_2O adsorption, with ΔE_{pol} and ΔE_{CT} being roughly equal over the entire range of distances. In other words, polarization contributes more to the total binding than for the adsorption of C_2H_4. While charge transfer is relatively more important for the top adsorption mode, it is still far from reaching the importance it takes for ethylene adsorption. We suggest that this "lower than expected" importance of charge transfer for the adsorption of CO on Pt(111) is due to the intricate donation and back-donation involved in CO adsorption, which can be seen as a particularly strong polarization effect. In other words, it is the polarization which is particularly strong for CO adsorption, not the charge transfer that is small: this dative bond is the strongest bond investigated herein, and orbital interactions are without any doubt key for its accurate description. However, our analysis demonstrates that the top site is more sensitive to charge transfer than adsorption on the hollow site. This is in good agreement with previous reports,[70] but it is the first time that

such a difference is clearly traced back to charge transfer and disentangled from polarization effects.

5. CONCLUSIONS

In this work, we have presented the extension of the BLW formalism to systems that require fractionally occupied orbitals such as metals at finite temperature. Since the computational cost of the rigorous combinatorial formulation is unpractical, our extension relies on a mean-field approximation to ensemble BLW in the context of mixed-state theory. This approximation is based on a new concept: selfish orbitals. Selfish orbitals are normalized, but their interactions with other orbitals are scaled down according to their occupation number. This mean-field approximation is exact in the case of infinitesimal smearing (i.e., BLW with a gap) and/or 1-block systems (i.e., ensemble KS-DFT). Furthermore, in numerical examples studied, the estimated error in the polarization energy is roughly 0.5 kcal mol^{-1}.

The method has been implemented in CP2K, and numerical applications have shown that H_2S is much more strongly bound to Pt(111) due to charge transfer, while the contribution of polarization is on a similar level as for H_2O. The chemisorption of ethylene on Pt(111) is, however, dominated by the charge transfer, and the two modes (di-σ and π) show the same type of bonding, with proportions of different interaction energy components close to the ones of H_2S. CO adsorption, on the other hand, is shown to depend significantly on the adsorption site: although the bond is five times stronger than for H_2O, the hollow-site adsorption is characterized by a roughly equal contribution of polarization and charge transfer, just like water adsorption. On the top site, charge transfer is somewhat more important, but even in this case, its importance is relatively smaller than for H_2S or C_2H_4. We ascribe this particularity to the donation/back-donation of CO, which can be seen as a particularly strong polarization contribution.

As demonstrated herein, BLW-EDA provides a convenient (i.e., easy to use) tool, providing polarization and charge-transfer energies at the metal interface, which is expected to provide valuable insight for catalysis and the understanding of the metal/gas and metal/liquid interface.

■ ASSOCIATED CONTENT

Ⓢ Supporting Information

The Supporting Information is available free of charge on the ACS Publications website at DOI: 10.1021/acs.jctc.8b00957.

> Density recovery; comparison of results with two different Pt pseudopotentials and results from VASP; further analysis of the deformation energy; influence of the electronic temperature; expanded Figures 2, 3, and 4; numerical results (PDF)

> Archive with optimized geometries and their opt-PBE-vdW energies as obtained by VASP (ZIP)

■ AUTHOR INFORMATION

Corresponding Author
*E-mail: stephan.steinmann@ens-lyon.fr.

ORCID Ⓘ
Marcella Iannuzzi: 0000-0001-9717-2527
Rustam Z. Khaliullin: 0000-0002-9073-6753
Stephan N. Steinmann: 0000-0002-2777-356X

■ ACKNOWLEDGMENTS

The authors thank J. Hutter for insightful discussions.

■ REFERENCES

(1) Heitler, W.; London, F. Wechselwirkung neutraler Atome und homo-polare Bindung nach der Quantenmechanik. *Eur. Phys. J. A* **1927**, *44*, 455−472.

(2) Ruedenberg, K. The Physical Nature of the Chemical Bond. *Rev. Mod. Phys.* **1962**, *34*, 326−376.

(3) Bader, R. F. W. *Atoms in Molecules: A Quantum Theory*; Oxford University Press: New York, 1990.

(4) Reed, A. E.; Curtiss, L. A.; Weinhold, F. Intermolecular interactions from a natural bond orbital, donor-acceptor viewpoint. *Chem. Rev.* **1988**, *88*, 899−926.

(5) Gonthier, J. F.; Steinmann, S. N.; Wodrich, M. D.; Corminboeuf, C. Quantification of "fuzzy" chemical concepts: a computational perspective. *Chem. Soc. Rev.* **2012**, *41*, 4671−4687.

(6) Tsipis, A. C. DFT challenge of intermetallic interactions: From metallophilicity and metallaromaticity to sextuple bonding. *Coord. Chem. Rev.* **2017**, *345*, 229−262.

(7) Pastorczak, E.; Corminboeuf, C. Perspective: Found in translation: Quantum chemical tools for grasping non-covalent interactions. *J. Chem. Phys.* **2017**, *146*, 120901.

(8) Philipsen, P. H. T.; Baerends, E. J. Role of the Fermi Surface in Adsorbate-Metal Interactions: An Energy Decomposition Analysis. *J. Phys. Chem. B* **2006**, *110*, 12470−12479.

(9) Cruz Hernandez, N.; Zicovich-Wilson, C. M.; Fdez. Sanz, J. The constrained space orbital variation analysis for periodic *ab initio* calculations. *J. Chem. Phys.* **2006**, *124*, 194105.

(10) Raupach, M.; Tonner, R. A periodic energy decomposition analysis method for the investigation of chemical bonding in extended systems. *J. Chem. Phys.* **2015**, *142*, 194105.

(11) Xin, H.; Linic, S. Analyzing relationships between surface perturbations and local chemical reactivity of metal sites: Alkali promotion of O2 dissociation on Ag(111). *J. Chem. Phys.* **2016**, *144*, 234704.

(12) Pecher, J.; Mette, G.; Durr, M.; Tonner, R. Site-Specific Reactivity of Ethylene at Distorted Dangling-Bond Configurations on Si(001). *ChemPhysChem* **2017**, *18*, 357−365.

(13) Pecher, J.; Schober, C.; Tonner, R. Chemisorption of a Strained but Flexible Molecule: Cyclooctyne on Si(001). *Chem. - Eur. J.* **2017**, *23*, 5459−5466.

(14) Mo, Y.; Song, L.; Wu, W.; Zhang, Q. Charge transfer in the electron donor-acceptor complex BH3NH3. *J. Am. Chem. Soc.* **2004**, *126*, 3974−3982.

(15) Khaliullin, R. Z.; Head-Gordon, M.; Bell, A. T. An efficient self-consistent field method for large systems of weakly interacting components. *J. Chem. Phys.* **2006**, *124*, 204105.

(16) Kaduk, B.; Kowalczyk, T.; Van Voorhis, T. Constrained Density Functional Theory. *Chem. Rev.* **2012**, *112*, 321−370.

(17) Plaisance, C. P.; van Santen, R. A.; Reuter, K. Constrained-Orbital Density Functional Theory. Computational Method and Applications to Surface Chemical Processes. *J. Chem. Theory Comput.* **2017**, *13*, 3561−3574.

(18) Mao, Y.; Ge, Q.; Horn, P. R.; Head-Gordon, M. On the Computational Characterization of Charge-Transfer Effects in Noncovalently Bound Molecular Complexes. *J. Chem. Theory Comput.* **2018**, *14*, 2401−2417.

(19) Stoll, H.; Wagenblast, G.; Preuss, H. On the use of local basis sets for localized molecular orbitals. *Theor. Chim. Acta* **1980**, *57*, 169−178.

(20) Gianinetti, E.; Raimondi, M.; Tornaghi, E. Modification of the Roothaan equations to exclude BSSE from molecular interaction calculations. *Int. J. Quantum Chem.* **1996**, *60*, 157−166.

(21) Nagata, T.; Takahashi, O.; Saito, K.; Iwata, S. Basis set superposition error free self-consistent field method for molecular interaction in multi-component systems: Projection operator formalism. *J. Chem. Phys.* **2001**, *115*, 3553−3560.

(22) Mo, Y.; Gao, J.; Peyerimhoff, S. D. Energy decomposition analysis of intermolecular interactions using a block-localized wave function approach. *J. Chem. Phys.* **2000**, *112*, 5530−5538.

(23) Khaliullin, R. Z.; Cobar, E. A.; Lochan, R. C.; Bell, A. T.; Head-Gordon, M. Unravelling the Origin of Intermolecular Interactions Using Absolutely Localized Molecular Orbitals. *J. Phys. Chem. A* **2007**, *111*, 8753−8765.

(24) Khaliullin, R. Z.; Bell, A. T.; Head-Gordon, M. Analysis of charge transfer effects in molecular complexes based on absolutely localized molecular orbitals. *J. Chem. Phys.* **2008**, *128*, 184112.

(25) Azar, R. J.; Head-Gordon, M. An energy decomposition analysis for intermolecular interactions from an absolutely localized molecular orbital reference at the coupled-cluster singles and doubles level. *J. Chem. Phys.* **2012**, *136*, 024103.

(26) Thirman, J.; Head-Gordon, M. An energy decomposition analysis for second-order M?ller-Plesset perturbation theory based on absolutely localized molecular orbitals. *J. Chem. Phys.* **2015**, *143*, 084124.

(27) Smits, G. F.; Krol, M. C.; van der Hart, W. J.; Altona, C. Theoretical investigations of the nature of intramolecular interactions. *Mol. Phys.* **1986**, *59*, 209−225.

(28) Mo, Y.; Wu, W.; Song, L.; Lin, M.; Zhang, Q.; Gao, J. The Magnitude of Hyperconjugation in Ethane: A Perspective from Ab Initio Valence Bond Theory. *Angew. Chem., Int. Ed.* **2004**, *43*, 1986−1990.

(29) Wodrich, M. D.; Gonthier, J. F.; Steinmann, S. N.; Corminboeuf, C. How Strained are Carbomeric-Cycloalkanes? *J. Phys. Chem. A* **2010**, *114*, 6705−6712.

(30) Levine, D. S.; Horn, P. R.; Mao, Y.; Head-Gordon, M. Variational Energy Decomposition Analysis of Chemical Bonding. 1. Spin-Pure Analysis of Single Bonds. *J. Chem. Theory Comput.* **2016**, *12*, 4812−4820.

(31) Levine, D. S.; Head-Gordon, M. Energy decomposition analysis of single bonds within Kohn−Sham density functional theory. *Proc. Natl. Acad. Sci. U. S. A.* **2017**, *114*, 12649−12656.

(32) Couty, M.; Bayse, C. A.; Hall, M. B. Extremely localized molecular orbitals (ELMO): a non-orthogonal Hartree-Fock method. *Theor. Chem. Acc.* **1997**, *97*, 96−109.

(33) Fornili, A.; Sironi, M.; Raimondi, M. Determination of extremely localized molecular orbitals and their application to quantum mechanics/molecular mechanics methods and to the study of intramolecular hydrogen bonding. *J. Mol. Struct.: THEOCHEM* **2003**, *632*, 157−172.

(34) Genoni, A.; Ghitti, M.; Pieraccini, S.; Sironi, M. A novel extremely localized molecular orbitals based technique for the one-electron density matrix computation. *Chem. Phys. Lett.* **2005**, *415*, 256−260.

(35) Fornili, A.; Moreau, Y.; Sironi, M.; Assfeld, X. On the suitability of strictly localized orbitals for hybrid QM/MM calculations. *J. Comput. Chem.* **2006**, *27*, 515−523.

(36) Genoni, A. X-ray Constrained Extremely Localized Molecular Orbitals: Theory and Critical Assessment of the New Technique. *J. Chem. Theory Comput.* **2013**, *9*, 3004−3019.

(37) Steinmann, S. N.; Jana, D. F.; Wu, J. I.-C.; Schleyer, P. v. R.; Mo, Y.; Corminboeuf, C. Direct Assessment of Electron Delocaliza-

tion Using NMR Chemical Shifts. *Angew. Chem., Int. Ed.* **2009**, *48*, 9828−9833.

(38) Elgabarty, H.; Khaliullin, R. Z.; Kuhne, T. D. Covalency of hydrogen bonds in liquid water can be probed by proton nuclear magnetic resonance experiments. *Nat. Commun.* **2015**, *6*, 8318.

(39) Steinmann, S. N.; Vogel, P.; Mo, Y.; Corminboeuf, C. The norbornene mystery revealed. *Chem. Commun.* **2011**, *47*, 227−229.

(40) Steinmann, S. N.; Mo, Y.; Corminboeuf, C. How do electron localization functions describe π-electron delocalization? *Phys. Chem. Chem. Phys.* **2011**, *13*, 20584−20592.

(41) Bomble, L.; Steinmann, S. N.; Perez-Peralta, N.; Merino, G.; Corminboeuf, C. Bonding analysis of planar hypercoordinate atoms via the generalized BLW-LOL. *J. Comput. Chem.* **2013**, *34*, 2242−2248.

(42) Mo, Y.; Gao, J. Polarization and Charge-Transfer Effects in Aqueous Solution via Ab Initio QM/MM Simulations. *J. Phys. Chem. B* **2006**, *110*, 2976−2980.

(43) Giese, T. J.; Chen, H.; Huang, M.; York, D. M. Parametrization of an Orbital-Based Linear-Scaling Quantum Force Field for Noncovalent Interactions. *J. Chem. Theory Comput.* **2014**, *10*, 1086−1098.

(44) Demerdash, O.; Mao, Y.; Liu, T.; Head-Gordon, M.; Head-Gordon, T. Assessing many-body contributions to intermolecular interactions of the AMOEBA force field using energy decomposition analysis of electronic structure calculations. *J. Chem. Phys.* **2017**, *147*, 161721.

(45) Bambagioni, V.; Bevilacqua, M.; Bianchini, C.; Filippi, J.; Lavacchi, A.; Marchionni, A.; Vizza, F.; Shen, P. K. Cover Picture: Self-Sustainable Production of Hydrogen, Chemicals, and Energy from Renewable Alcohols by Electrocatalysis (ChemSusChem 7/ 2010). *ChemSusChem* **2010**, *3*, 765−765.

(46) Liu, P.; Norskov, J. K. Ligand and ensemble effects in adsorption on alloy surfaces. *Phys. Chem. Chem. Phys.* **2001**, *3*, 3814−3818.

(47) Gianinetti, E.; Vandoni, I.; Famulari, A.; Raimondi, M. Extension of the SCF-MI method to the case of K fragments one of which is an open-shell system. *Adv. Quantum Chem.* **1998**, *31*, 251−266.

(48) Horn, P. R.; Sundstrom, E. J.; Baker, T. A.; Head-Gordon, M. Unrestricted absolutely localized molecular orbitals for energy decomposition analysis: Theory and applications to intermolecular interactions involving radicals. *J. Chem. Phys.* **2013**, *138*, 134119.

(49) Yang, W.; Mori-Sanchez, P.; Cohen, A. J. Extension of many-body theory and approximate density functionals to fractional charges and fractional spins. *J. Chem. Phys.* **2013**, *139*, 104114.

(50) Steinmann, S. N.; Yang, W. Wave function methods for fractional electrons. *J. Chem. Phys.* **2013**, *139*, 074107.

(51) Khaliullin, R. Z.; VandeVondele, J.; Hutter, J. Efficient Linear-Scaling Density Functional Theory for Molecular Systems. *J. Chem. Theory Comput.* **2013**, *9*, 4421−4427.

(52) Mayer, I.; Surjan, P. R. Localization and delocalization. II. Role of overlap in interbond interactions. *J. Chem. Phys.* **1984**, *80*, 5649−5658.

(53) *CP2K Open Source Molecular Dynamics*, available at https://www.cp2k.org/.

(54) Kresse, G.; Hafner, J. Ab initio molecular dynamics for liquid metals. *Phys. Rev. B: Condens. Matter Mater. Phys.* **1993**, *47*, 558.

(55) Kresse, G.; Furthmuller, J. Efficient iterative schemes for ab initio total-energy calculations using a plane-wave basis set. *Phys. Rev. B: Condens. Matter Mater. Phys.* **1996**, *54*, 11169.

(56) Klimes, J.; Bowler, D. R.; Michaelides, A. Chemical accuracy for the van der Waals density functional. *J. Phys.: Condens. Matter* **2010**, *22*, 022201.

(57) Steinmann, S. N.; Corminboeuf, C. Comprehensive Benchmarking of a Density-Dependent Dispersion Correction. *J. Chem. Theory Comput.* **2011**, *7*, 3567−3577.

(58) Gautier, S.; Steinmann, S. N.; Michel, C.; Fleurat-Lessard, P.; Sautet, P. Molecular adsorption at Pt(111). How accurate are DFT functionals? *Phys. Chem. Chem. Phys.* **2015**, *17*, 28921−28930.

(59) Blochl, P. E. Projector augmented-wave method. *Phys. Rev. B: Condens. Matter Mater. Phys.* **1994**, *50*, 17953.

(60) Kresse, G.; Joubert, D. From ultrasoft pseudopotentials to the projector augmented-wave method. *Phys. Rev. B: Condens. Matter Mater. Phys.* **1999**, *59*, 1758.

(61) VandeVondele, J.; Hutter, J. Gaussian basis sets for accurate calculations on molecular systems in gas and condensed phases. *J. Chem. Phys.* **2007**, *127*, 114105.

(62) Goedecker, S.; Teter, M.; Hutter, J. Separable dual-space Gaussian pseudopotentials. *Phys. Rev. B: Condens. Matter Mater. Phys.* **1996**, *54*, 1703−1710.

(63) Boys, S. F.; Bernardi, F. The calculation of small molecular interactions by the differences of separate total energies. Some procedures with reduced errors. *Mol. Phys.* **1970**, *19*, 553−566.

(64) Steinmann, S. N.; Corminboeuf, C.; Wu, W.; Mo, Y. Dispersion-Corrected Energy Decomposition Analysis for Intermolecular Interactions Based on the BLW and dDXDM Methods. *J. Phys. Chem. A* **2011**, *115*, 5467−5477.

(65) Bondi, A. van der Waals Volumes and Radii. *J. Phys. Chem.* **1964**, *68*, 441−451.

(66) Miller, T. M. *CRC Handbook of Chemistry and Physics*; Taylor & Francis Group: Boca Raton, FL, 2010.

(67) Reed, A. E.; Schleyer, P. v. R. Chemical bonding in hypervalent molecules. The dominance of ionic bonding and negative hyperconjugation over d-orbital participation. *J. Am. Chem. Soc.* **1990**, *112*, 1434−1445.

(68) Steinmann, S. N.; Fleurat-Lessard, P.; Gotz, A. W.; Michel, C.; Ferreira de Morais, R.; Sautet, P. Molecular mechanics models for the image charge, a comment on "Including image charge effects in the molecular dynamics simulations of molecules on metal surfaces. *J. Comput. Chem.* **2017**, *38*, 2127−2129.

(69) Steinmann, S. N.; Ferreira De Morais, R.; Gotz, A. W.; Fleurat-Lessard, P.; Iannuzzi, M.; Sautet, P.; Michel, C. Force Field for Water over Pt(111): Development, Assessment, and Comparison. *J. Chem. Theory Comput.* **2018**, *14*, 3238−3251.

(70) Kalhara Gunasooriya, G. T. K.; Saeys, M. CO Adsorption Site Preference on Platinum: Charge Is the Essence. *ACS Catal.* **2018**, *8*, 3770−3774.